

# ROME: Robustifying Memory-Efficient NAS via Topology Disentanglement and Gradients Accumulation

Xiaoxing Wang<sup>1†\*</sup>    Xiangxiang Chu<sup>2†</sup>    Yuda Fan<sup>1\*</sup>    Zhexi Zhang<sup>1</sup>    Xiaolin Wei<sup>2</sup>

Junchi Yan<sup>1\*</sup>    Xiaokang Yang<sup>1</sup>

<sup>1</sup>Shanghai Jiao Tong University, <sup>2</sup>Meituan

{figure1\_wxx, kurodakanbei, jerseyzhang, yanjunchi, xkyang}@sjtu.edu.cn

{chuxiangxiang, weixiaolin02}@meituan.com

## Abstract

*Single-path based differentiable neural architecture search has great strengths for its low computational cost and memory-friendly nature. However, we surprisingly discover that it suffers from severe searching instability which has been primarily ignored, posing a potential weakness for a wider application. In this paper, we delve into its performance collapse issue and propose a new algorithm called RObustifying Memory-Efficient NAS (ROME). Specifically, 1) for consistent topology in the search and evaluation stage, we involve separate parameters to disentangle the topology from the operations of the architecture. In such a way, we can independently sample connections and operations without interference; 2) to discount sampling unfairness and variance, we enforce fair sampling for weight update and apply a gradient accumulation mechanism for architecture parameters. Extensive experiments demonstrate that our proposed method has strong performance and robustness, where it mostly achieves state-of-the-art results on a large number of standard benchmarks.*

## 1. Introduction

Despite the fast development of neural architecture search (NAS) [41] to aid network design in vision tasks like classification [29], object detection [13], and segmentation [20], there has been an urging demand for faster searching algorithms. Early methods based on massive evaluation of candidate models [41, 28, 15] require unaffordable costs (typically 2K GPU days). In the light of weight-sharing

mechanism introduced in SMASH [4], a variety of low-cost approaches have emerged [3, 25, 22]. Differentiable architecture search [22] has taken the dominance with a myriad of follow-up works [31, 5, 32, 12, 7, 37]. In this paper, we investigate the single-path based branch [12] for its efficiency that only requires a single path in memory.

Unlike many DARTS variants that have to perform all candidate operations, single-path based methods [27, 12, 32], also termed as memory-efficient NAS<sup>1</sup>, are developed to sample and activate one operation from each edge. Specifically, the Gumbel-Softmax reparameterization tricks [16, 23] are employed to achieve differentiable and memory-efficient search [31, 12, 32].

In this paper, we discover that existing single-path based searching methods yet suffer a severe instability problem, upon which we propose a novel algorithm to disentangle the search for optimal topology (i.e. edge connections) from operation choices. Specifically, in addition to parameters  $\alpha$  representing the importance of operations, we involve topology parameters  $\beta$  to represent the relative importance of edges. A single-path architecture is induced by independently sampling candidate connections and operations based on  $\beta$  and  $\alpha$  respectively. Moreover, to robustify the training of operation weights and architecture parameters, we propose a gradient accumulation strategy during the bi-level optimization. In a nutshell, our contributions are:

**1) Deep dive into the collapse in single-path based NAS.** We discover that single-path based methods also suffer from the instability issue. Similar to the performance collapse problem in DARTS that has been discussed in recent works [38, 6, 32, 19], the architectures searched by single-path based methods can also be dominated by pa-

\*Correspondent author. † Equal contribution. \* Work done as an intern in Meituan.

<sup>1</sup>In this paper, we interchangeably use the term ‘single-path’ and ‘memory-efficient’ for describing such kinds of NAS methods.

parameterless operations, especially skip connections. This motivates us to scheme techniques to improve its stability.

**2) Consistent search and evaluation by disentangling topology search from operation selection.** Independent topological distribution is designed to achieve consistent architecture between the search and inference stage, which separates the search for optimal topology from operations. To our best knowledge, this is the first work to achieve consistent search and evaluation for single-path based differentiable NAS, though there are counterpart techniques like edge normalization [33] developed in the full-path scenario.

**3) Robustifying bi-level optimization via gradient accumulation.** Compared with the full-path methods whereby all the operations are involved for training, the instability issue by the random sampling of operations in the single-path methods can be more pronounced. We propose to accumulate the gradients over sampling iterations to acquire more stable gradient estimation, for both architecture parameters and network weights. Our work is one of the first attempts to address the stability issue during the bi-level optimization of single-path based NAS.

**4) Strong performance while maintaining low memory cost.** Our memory-efficient approach achieves state-of-the-art on various search spaces and datasets across 15 benchmarks. We will provide the source code and hyperparameter settings to make our work reproducible.

## 2. Related Work

**Differentiable Neural Architecture Search.** Similar to [42, 25] that uses a directed acyclic graph to represent a cell, DARTS [22] constructs a cell-based supernet and further introduces architecture parameters to represent the importance of each operation. It formulates the searching process as a bi-level optimization problem [1]. DARTS proposes two types (first-order and second-order) of approximation that alternatively update network weights and architecture parameters with stochastic gradient descent. However, since the supernet subsumes all connections and operations within the search space, DARTS risks exhausting the memory when searching for a larger network. In this regard, DARTS searches for a smaller network as a proxy and then increases the depth to have a large model in the evaluation stage. A possible attempt to resolve this issue is done by progressively pruning the operations and gradually increasing the depths [7], which is still an indirect approach and requires strong regularization tricks. Apart from that, recent works [38, 6] also point out an instability phenomenon of DARTS. These issues significantly restrict its application.

**Memory-efficient NAS.** To reduce the memory cost, several prior works revise the forward procedure of a supernet. PC-DARTS [33] makes use of partial connections instead of the full-fledged supernet. MergeNAS [30] proposes to merge all parametric operations into one convolution, a

similar super-kernel strategy is also used in [27]. Proxyless-NAS [5] samples two paths instead of all paths during the search process, which enables proxyless searching on large datasets. Single-path based supernets [14, 8] sample only a single path at each iteration, which are two-stage methods that require additional searching to choose the final models. GDAS [12] sample a subgraph of the DAG at each iteration, which is by far the most efficient. However, we observe that a severe instability issue occurs when applying a single-path based differentiable method, which previously has been neglected.

**Performance collapse of DARTS.** The collapse issue is one of the most critical problems in differentiable architecture search [19, 33, 9, 6, 38]. It has been shown that DARTS [22] prefers to choose the parameterless operations, leading to its performance collapse [19, 9]. Recent works [38, 6] utilize the eigenvalue of the Hessian matrix as an indicator of collapse and design various techniques to regularize high eigenvalues. Instead, [19, 7] directly constricts the number of skip connections to 2 to step aside the collapse. Nonetheless, the previous methods are specifically designed for the full-path training scheme. Whereas the collapse problem in single-path mode has been rarely studied. Our method addresses this issue with a simplistic sampling technique, which preserves the memory-friendly feature. We believe our effort is a promising direction towards efficient and stable NAS.

## 3. Methodology

We first introduce the preliminary of differentiable single-path methods [12, 11] that exploit Gumbel reparameterization, and next we disclose a new collapse. We dive into its cause, propose our method, and discuss its strengths.

### 3.1. Review on Differentiable Single-Path Methods

DARTS [22] optimizes a supernet stacked by normal cells and reduction cells. A cell is represented by a DAG with  $N$  nodes  $\{x_i\}_{i=1}^N$  where each node  $x_i$  denotes latent representation. Edge  $e_{i,j}$  from node  $x_i$  to  $x_j$  integrates all the candidate operations  $\mathcal{O}$ , and the output  $\bar{o}_{i,j}(x_i)$  is:

$$\bar{o}_{i,j}(x_i) = \sum_{o \in \mathcal{O}} \frac{\exp(\alpha_{i,j}^o)}{\sum_{o' \in \mathcal{O}} \exp(\alpha_{i,j}^{o'})} o(x_i), \quad (1)$$

where  $\alpha_{i,j}^o$  is the architecture weight for operation  $o(x_i)$ , as the operation importance. Each intermediate node is connected by all of its predecessors:  $x_j = \sum_{i < j} \bar{o}_{i,j}(x_i)$ .

Different from the compound operation in Eq. 1, single-path methods construct a memory-efficient structure. For edge  $e_{i,j}$ , a one-hot random vector  $z_{i,j} \in \mathbb{R}^{|\mathcal{O}|}$  is sampled. Based on the sampled  $z_{i,j}$ , only one candidate operation is

selected during the forward pass:

$$\bar{o}_{i,j}(x_i) = \sum_{o \in \mathcal{O}} z_{i,j}^o \cdot o(x_i), \quad (2)$$

where  $z_{i,j}^o$  equals to 1 if the operation  $o$  is sampled otherwise 0.

To distinguish the most important operations, DARTS uses a bi-level optimization by alternately updating the operation parameters  $\theta$  and architecture weights  $\alpha$ . Since the weights of all operations are involved, DARTS is memory-consuming. This is addressed by differentiable single-path methods where one out of all operations is sampled and activated at each iteration. [12, 31, 32] utilize Gumbel-Softmax reparameterization to make the sampling procedure differentiable, and adopt a bi-level optimization,

$$\begin{aligned} \alpha &\leftarrow \alpha - \nabla_{\alpha} L_{val}(\theta_z, \alpha), \\ \theta_{z'} &\leftarrow \theta_{z'} - \nabla_{\theta_{z'}} L_{train}(\theta_{z'}, \alpha), \end{aligned} \quad (3)$$

where  $z, z' \sim p(z|\alpha)$  indicates the activated architectures sampled under a distribution determined by the architecture weights  $\alpha$ , and  $\theta_z$  indicates the selected operation weights in the architecture  $z$ .

The main difference between GDAS [12] and SNAS [32] is that the former provides a memory-efficient version by activating paths in a one-hot way. Note that the normal cell of the best model found in [12] has 4 skip connections. And for GDAS (FRC), the normal cell contains 5 skip connections. These observations motivate us to dive into whether there is performance collapse like DARTS found in recent works [38, 9, 6, 40]. Therefore, we rerun the released code [12] to search several times, where the found normal cells are composed of almost all parameterless operations such as skip connection and max pooling, shown in Fig. 1. It resembles the collapse problem in DARTS, so we also call this phenomenon **performance collapse**. However, the cause of it in a single-path based method differs from that in DARTS.

On one hand, for the fourth intermediate node, its output is generated by integrating the output of five paths, which brings more difficulties to optimize and thus slows down the convergence of searching loss. Once skip connection is selected during the sampling process, it is beneficial to faster loss descent, which in turn increases  $\alpha_{skip}$  and makes it eventually dominate the architecture parameters.

On the other hand, unlike the sampling scheme that each edge owns one operation in the search phase, the final model is inferred by only preserving two input edges for each node. Such a difference in network topology can mislead the searching objective.

In general, we address this collapse by focusing on two issues: inconsistency between the searching and inferring stage, and instability of the bi-level optimization.

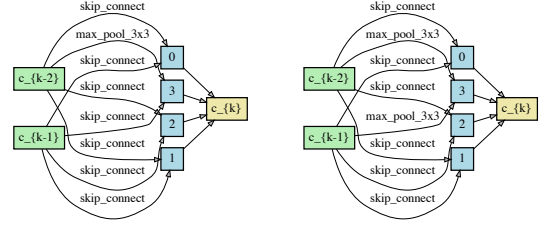


Figure 1. Two failure examples of GDAS [12] in the DARTS search space produced in our experiment by running the authors’ code, where normal cells are full of parameterless operations.

### 3.2. Root Analysis for Single-Path NAS Collapse

**Inconsistency between the searching and inferring stage.** For one-shot NAS, the structure inconsistency between supernet and final network is mainly reflected in both operation-level and topology-level. The operation-level inconsistency has been alleviated in recent single-path based methods [12, 32] by sampling one operation on each edge at each iteration in the search phase. However, the topology-level inconsistency issue is neglected. Specifically, nodes in the supernet connect with all its predecessors, while nodes in the final network only have two in-degrees.

In this paper, we propose to eliminate the search-evaluation inconsistency at both operation and topology level by disentangling the search for topology and operations. Simultaneously, our proposed approach is even more memory-efficient due to less storage and computation cost.

**Instability of the stochastic bi-level optimization.** Instability issues for single-path based methods can result from its stochastic nature that involves sub-sampling. Specifically, only a subset of operations is sampled at each iteration, resulting in insufficient training of weights  $\theta$  and  $\alpha$ . Additionally, the final architecture is inferred by the architecture parameters  $\alpha$ , while the sampling scheme involves high variance for the gradient of  $\alpha$ , affecting the convergence of searching. Therefore, it is critical to stabilize such a challenging optimization procedure.

To achieve more accurate estimation and reduce the approximation variance, we propose accumulating and averaging the gradients of architecture parameters.

### 3.3. Disentanglement of the Search for Topology

To disentangle the search for topology and operations on each edge, we use an indicator  $B_{i,j} \in \{0, 1\}$  to denote whether edge  $e_{i,j}$  is selected, and  $A_{i,j}^o \in \{0, 1\}$  to denote whether operation  $o$  is selected given edge  $e_{i,j}$ . The probability of selecting connection  $z_{i,j}^o$  can be formulated as:

$$p(z_{i,j}^o = 1) = p(B_{i,j} = 1)p(A_{i,j}^o = 1). \quad (4)$$

Therefore, sampling architecture  $z$  with  $M$  connections can be decomposed into two parts: independently sample  $M$

candidate edges and their operations.

**Sampling for operations.** To sample operation on each edge, we follow Eq. 1 and use Gumbel-Max [12, 32]:

$$\tilde{\alpha}_{i,j}^o = \frac{\exp(\alpha_{i,j}^o)}{\sum_{o' \in \mathcal{O}} \exp(\alpha_{i,j}^{o'})}, \quad (5)$$

$$\mathbf{A}_{i,j} = \text{one\_hot} \left[ \arg \max_{o \in \mathcal{O}} (\log \tilde{\alpha}_{i,j}^o + \mathbf{g}_{i,j}^o) \right] \in \mathbb{R}^{|\mathcal{O}|}, \quad (6)$$

where  $\mathbf{g}_{i,j}^o$  are i.i.d. samples drawn from Gumbel (0,1) distribution<sup>2</sup>.  $\mathbf{A}_{i,j}$  is the one-hot vector indicating which operation is selected on  $e_{i,j}$ . As  $\tilde{\alpha}_{i,j}^o$  is the probability of the operator being chosen among all the operators on edge  $e_{i,j}$ , we have:

$$p(z_{i,j}^o) = \tilde{\alpha}_{i,j}^o = p(\mathbf{A}_{i,j}^o = 1). \quad (7)$$

To make search objective differentiable to operation parameter  $\alpha$ , we relax the discrete distribution to a continuous one by Gumbel-Softmax:

$$\tilde{\mathbf{A}}_{i,j}^o = \frac{\exp \left[ (\log \tilde{\alpha}_{i,j}^o + \mathbf{g}_{i,j}^o) / \tau \right]}{\sum_{o'=1}^{|\mathcal{O}|} \exp \left[ (\log \tilde{\alpha}_{i,j}^{o'} + \mathbf{g}_{i,j}^{o'}) / \tau \right]},$$

$$\mathbf{A}_{i,j} = \text{one\_hot} \left[ \arg \max_{o \in \mathcal{O}} \tilde{\mathbf{A}}_{i,j}^o \right], \quad (8)$$

in which  $\tau$  is the temperature that gradually decreases during the searching stage.

**Sampling for edges.** As analyzed in Sec. 3.2, topology inconsistency issue occurs in the prior single-path based methods [12, 32], where all 14 edges in a cell are selected in the search stage but only 8 edges are retained in the inferring stage. To eliminate such an inconsistency issue, we propose an end-to-end method, referred to as ROME, to directly search the target model, which means sampling 8 edges per cell during the search session as well.

Each intermediate node should connect with exact two predecessors, satisfying DARTS's constraints on the cell topology:

$$\sum_{i < j} \mathbf{B}_{i,j} = 2, \quad \forall j. \quad (9)$$

Specifically, we introduce two versions of ROME based on different edge sampling ideas: ROME-v1 and ROME-v2.

**1) ROME-v1.** Suppose node  $x_j$  has  $j$  possible predecessors to connect to, there exists  $\frac{j \times (j-1)}{2}$  types of edge selection. We introduce  $\mathbf{I}_j^{(i,k)}$ ,  $i < k < j$  to indicate if node  $x_j$  is connected to  $x_i$  and  $x_k$ . When  $\mathbf{I}_j^{(i,k)} = 1$ , we have:

$$\mathbf{B}_{m,j} = \begin{cases} 1, & m = i \text{ or } m = k \\ 0, & \text{otherwise} \end{cases}. \quad (10)$$

<sup>2</sup> $\mathbf{g}_{i,j}^o = -\log(-\log(\mathbf{u}_{i,j}^o))$ ,  $\mathbf{u}_{i,j}^o$  is drawn from uniform distribution

We then set a trainable variable  $\beta_j^{(i,k)}$  to denote the intensity of each edge selection case for node  $x_j$ .

$$p\left(\mathbf{I}_j^{(i,k)} = 1\right) = \frac{\exp(\beta_j^{(i,k)})}{\sum_{i' < k' < j} \exp(\beta_j^{(i',k')})} \triangleq \tilde{\beta}_j^{(i,j)}. \quad (11)$$

Gumbel-Max reparameterization is also applied, where  $\mathbf{g}_j^{(i,k)}$  are i.i.d. samples from Gumbel (0,1) distribution:

$$\mathbf{I}_j = \text{one\_hot} \left[ \arg \max_{i < k < j} (\log \tilde{\beta}_j^{(i,k)} + \mathbf{g}_j^{(i,k)}) \right] \in \mathbb{R}^{\frac{j \times (j-1)}{2}}. \quad (12)$$

Taking the whole cell into consideration, if edge  $e_{i,j}$  is chosen, there must exist another chosen edge  $e_{k,j}$ , thus leading to

$$\mathbf{B}_{i,j} = \sum_{k < i} \mathbf{I}_j^{(k,i)} + \sum_{k > i} \mathbf{I}_j^{(i,k)}. \quad (13)$$

Intending to retain the gradient information, Gumbel-Softmax reparameterization is employed again:

$$\tilde{\mathbf{I}}_j^{(i,k)} = \frac{\exp \left\{ \left[ \log \tilde{\beta}_j^{(i,k)} + \mathbf{g}_j^{(i,k)} \right] / \tau \right\}}{\sum_{i' < k' < j} \exp \left\{ \left[ \log \tilde{\beta}_j^{(i',k')} + \mathbf{g}_j^{(i',k')} \right] / \tau \right\}},$$

$$\mathbf{I}_j = \text{one\_hot} \left[ \arg \max_{i < k < j} \tilde{\mathbf{I}}_j^{(i,k)} \right]. \quad (14)$$

In ROME-v1, we utilize 40 variables to represent the topology of normal and reduction cells because 4 intermediate nodes in a cell have 2, 3, 4, 5 predecessors respectively. By applying Gumbel-Softmax on operation and topology levels, we construct the target model efficiently instead of adding considerable extra parameters to learn.

**2) ROME-v2.** Different from ROME-v1 that utilizes  $\sum_{i=2}^{N+2} \binom{i}{2}$  variables to represent the topology of a cell with  $N$  intermediate nodes and two input nodes, ROME-v2 introduces the probability of selecting edge  $e_{i,j}$  as  $p(e_{i,j})$ , which can be calculated as follows:

$$p(e_{i,j}) = \frac{\exp(\beta_{i,j})}{\sum_{k < j} \exp(\beta_{k,j})} \triangleq \tilde{\beta}_{i,j}, \quad (15)$$

where  $\beta_{k,j}$  is the topology parameter. To satisfy the constraints on the cell topology (Eq. 9), ROME-v2 extends Gumbel-Max reparameterization to a Gumbel-Top2 trick:

$$\tilde{\mathbf{B}}_{i,j} = \frac{\exp \left( (\log \tilde{\beta}_{i,j} + \mathbf{g}_{i,j}) / \tau \right)}{\sum_{i' < j} \exp \left( (\log \tilde{\beta}_{i',j} + \mathbf{g}_{i',j}) / \tau \right)}, \quad (16)$$

$$\mathbf{B}_{i,j} = \begin{cases} 1, & i \in \arg \text{top2}_{i' < j}(\tilde{\mathbf{B}}_{i',j}) \\ 0, & \text{otherwise} \end{cases}. \quad (17)$$

ROME-v2 provides an efficient way to sample edges, and only 28 variables are used to represent the topology of normal and reduction cell with 4 intermediate nodes.

**Theoretical analysis on Gumbel-Top2.** We show that our Gumbel-Top2 technique is equivalent to sampling two different edges without replacement with probability simplex  $p_i$ . We sketch our proof as follows and the rigorous full version can be found in supplemental materials.

Let  $p_i$  be the probability of  $e_i$  being selected by single choice among  $n$  edges. Without loss of generality, we suppose that  $e_1$  is chosen.

i) Consider sampling two edges without replacement:

The probability of  $e_i$  being sampled is  $p_1 + \sum_{i=2}^n p_i \frac{p_1}{1-p_i}$ .

ii) Consider the Gumbel-Top2 scheme:

$\epsilon_i$  is sampled uniformly from  $[0, 1]$  and the largest two  $\log p_i - \log(-\log \epsilon_i)$ s are chosen. The cases that  $p_1$  is chosen can be divided into two disjoint parts.

**A)**  $\log p_1 - \log(-\log \epsilon_1)$  is the largest, and the probability is  $p_1$  due to our knowledge of Gumbel-Max scheme.

**B)**  $\log p_i - \log(-\log \epsilon_i)$  is the second largest only next to  $\log p_1 - \log(-\log \epsilon_1)$ . We directly get its probability:

$$\begin{aligned} & \int_0^1 \epsilon_1^{p_2/p_1} \epsilon_1^{p_3/p_1} \dots (1 - \epsilon_1^{p_i/p_1}) \dots \epsilon_1^{p_n/p_1} d\epsilon_1 \\ &= \int_0^1 (1 - \epsilon_1^{p_i/p_1}) \epsilon_1^{\frac{1-p_i}{p_1}-1} d\epsilon_1 \\ &= \frac{p_1}{1-p_i} - p_1 = p_i \frac{p_1}{1-p_i}. \end{aligned}$$

Therefore, the probability is  $p_1 + \sum_{i=2}^n p_i \frac{p_1}{1-p_i}$ , which means the two schemes are equivalent.

### 3.4. Gradient Summation in Bi-level Optimization

The single-path based GDAS [12] borrows DARTS’s bi-level optimization. It samples one architecture and applies one-step gradient descent to update operation parameters and architecture weights alternately. Fig. 1 shows this procedure can incur instability.

In our analysis, the sampling variance can mislead the architecture parameters. Moreover, insufficient training for weights of parametric operations should be considered since only the selected operations contribute to the network output, and other operations have no gradient. Consequently, we propose a gradient accumulation strategy to robustify the bi-level optimization.

As shown in Sec. 3.3, we utilize architecture weights  $\alpha$  and  $\beta$  to construct a parametric distribution. We select a candidate architecture by independently sampling edges and operations. Suppose there are  $M$  edges  $\{e_1, \dots, e_M\}$  and the corresponding operations  $\{o_1, \dots, o_M\}$  make up an architecture  $z = \{(e_1, o_1), \dots, (e_M, o_M)\}$ , and thus the probability of  $z$  being selected is given by:

$$p(z; \alpha, \beta) = \prod_{i=1}^M p(e_i; \beta) \times p(o_i | e_i; \alpha). \quad (18)$$

---

**Algorithm 1** ROME (with two versions v1 and v2).

---

**Input:** iteration count  $T$ ; number of sampling  $K$ ; initialized network weights  $\theta$ ; and architecture parameters  $\alpha, \beta$ ;

**Output:** optimal architecture  $z^*$ ;

```

1: for  $t = 1 \rightarrow T$  do
2:   Sample two batches of data samples  $D_s$  and  $D_t$ ;
3:   for  $k = 1 \rightarrow K$  do
4:     Operation sampling by Eq. 3.3;
5:     Topology sampling for search-evaluation consistency by Eq. 13 (for v1) or Eq. 17 (for v2);
6:     Get sampled architecture  $z_k$ ;
7:   end for
8:   Gradient accumulation and update  $\alpha, \beta$  by Eq. 20;
9:   for  $k = 1 \rightarrow K$  do
10:    Operation sampling by Eq. 3.3;
11:    Topology sampling for search-evaluation consistency by Eq. 13 (for V1) or Eq. 17 (for v2);
12:    Get sampled architecture  $z'_k$ ;
13:   end for
14:   Gradient accumulation and update  $\theta$  by Eq. 21;
15: end for
16: return:  $z^* = \arg \max_z p(z; \alpha, \beta)$ 

```

---

NAS can be then modeled as finding optimal  $\alpha$  and  $\beta$  to minimize the expectation of validation loss of the architectures as Eq. 19, where  $\theta_z^*$  denotes the optimal operation parameters for the sampled architecture  $z$ .

$$\begin{aligned} & \min_{\alpha, \beta} \mathbb{E}_{z \sim p(z; \alpha, \beta)} [L_{val}(\theta_z^*, z)] \\ & \text{s.t. } \theta_z^* = \arg \min_{\theta} L_{train}(\theta, z) \end{aligned} \quad (19)$$

Rather than GDAS [12] that approximates the expectation by sampling once, we propose to sample for  $K$  times and utilize the average loss to approximate the expectation. Suppose that the gradient of  $\alpha$  is a random variable with a variance of  $\sigma^2$ , sampling  $K$  times and averaging generate an unbiased estimator with a variance of  $\frac{\sigma^2}{K}$ . To make the average loss differentiable to architecture weights, we refer to DARTS [22] and use current  $\theta_z$  to approximate  $\theta_z^*$ .

Accordingly, we propose to train operation parameters by accumulating the gradients of operation weights under multiple candidate architectures. Not only gradient accumulation is able to alleviate the issue of insufficient training for operation parameters, but also it makes the approximation of  $\theta_z^*$  much more stable. Consequently, we can alternately update operation parameters  $\theta$  and architecture pa-

rameters  $\alpha$  (similar for  $\beta$ ) as:

$$\alpha \leftarrow \alpha - \frac{1}{K} \sum_{k=1}^K \nabla_{\alpha} L_{val}(\theta, z_k), \quad (20)$$

$$\theta \leftarrow \theta - \sum_{k=1}^K \nabla_{\theta} L_{train}(\theta, z'_k), \quad (21)$$

where  $z_k, z'_k, k = 1, \dots, K$  denote the sampled architectures. The overall method is shown in Alg. 1

## 4. Experiments

### 4.1. Protocols

**S0 (DARTS’s search space).** DARTS’s search space is comprised of a stack of duplicate normal cells and reduction cells. Each cell is represented by a DAG of 4 intermediate nodes. There are candidate operations {maxpool, avgpool, skip\_connect, sep\_conv 3×3 and 5×5, dil\_conv 3×3 and 5×5}, between each two nodes. We search and evaluate on both CIFAR-10 [17] and ImageNet [10].

**S1-S4 (RobustDARTS’s reduced search space).** We also conduct experiments on the reduced search spaces introduced by RobustDARTS [38]. S1 is a pre-optimized search space and the two candidate operations on each edge is different, see [38] for details. In other three search spaces, the candidate operations on each edge are the same. Specifically, S2 has {3 × 3 SepConv, SkipConnect}, S3 has {3 × 3 SepConv, SkipConnect, Zero (None)}, and S4 has {3 × 3 SepConv, Noise}. To demonstrate the robustness of our method, we search and evaluate under the above four search spaces on CIFAR-10, CIFAR-100 [17], and SVHN [24].

**Search settings.** Similar to DARTS, the supernet consists of 8 cells with 16 initial channels. We alternately update operation parameters and architecture weights for 50 epochs and set the sampling number  $K = 7$  by default. For operation parameters, we use the SGD optimizer with 0.9 momentum and set the base learning rate 0.05; For architecture weights, we adopt Adam optimizer and set the base learning rate  $3 \times 10^{-4}$ .

**Evaluation settings.** We use standard evaluation settings as DARTS [22]. Specially, we train the inferred model for 600 epochs using SGD with a batch size of 96. For S0 search space, networks are constructed by stacking 20 cells with 36 initial channels, and are trained with the same strategy and data processing tricks as the previous works [7, 22]. For S1-S4 search spaces, we strictly follow the settings in RobustDARTS [38] for fair comparison. We also increase the number of cells and initial channels to 20 and 36 as in SDARTS [6] for further evaluation.

### 4.2. Ablation Study

Our method disentangles the search for topology and utilizes gradient accumulation strategy to resolve the search-

Disentanglement	GA for $\theta$	Avg for $\alpha$	Acc (%)
×	×	×	96.52±0.07
✓	×	×	97.12±0.06
✓	×	✓	97.22±0.07
✓	✓	×	97.34±0.07
✓	✓	✓	<b>97.42±0.07</b>

Table 1. Component analysis of our method as searched and evaluated on CIFAR-10. We conduct three parallel tests on each setting and report the mean and standard deviation of top-1 accuracy.

# Samples ( $K$ )	Acc (%)	# Params (M)
1	97.12±0.06	3.34
4	97.28±0.07	3.57
7	97.42±0.07	3.73
10	97.46±0.12	4.06

Table 2. Sensitivity study of sampling number  $K$ . We do three parallel tests on each setting and report mean and standard deviation of top-1 accuracy. Models are searched and evaluated on CIFAR-10. The disentanglement technique is used in search phase.

evaluation inconsistency issue and alleviate the instability issue for single-path based methods. To show the efficacy of each component, we conduct an ablation study under S0 search space on CIFAR-10.

**Component analysis for the instability issue.** To evaluate how each component contributes to the instability issue, we utilize the disentanglement and gradient accumulation strategy separately. Results are shown in Table 1, where ‘GA for  $\theta$ ’ indicates applying gradient accumulation when training the network weights, ‘Avg for  $\alpha$ ’ indicates sampling candidate architectures for  $K = 7$  times and utilize the average loss to approximate the expectation. We observe that disentanglement can significantly improve the searching performance, indicating that the inconsistency issue is the principal reason for performance collapse. On one hand, inconsistent topology between search and evaluation results in inconsistent search objective; On the other hand, training weights of 14 operations (without disentanglement) is much more difficult than training 8 operations (with disentanglement), making the convergence slower. Moreover, we observe that gradient accumulation strategy on  $\theta$  and  $\alpha$  can both improve the search performance.

**Sensitivity to the sampling number  $K$ .** Table 2 compares accuracy by setting  $K$  as 1, 4, 7, 10. The average performance increases monotonically with  $K$  but saturates when  $K=7$ . Therefore, we use  $K=7$  by default.

**Memory analysis.** Table 3 compares GPU memory cost under S0 search space on CIFAR-10. ROME has the lowest memory cost and this advantage can be signified given more candidate operations in search space.

### 4.3. Search Results Analysis

**Result on CIFAR-10.** We conduct 4 parallel tests by searching with different random seeds and then evaluating

Method	DARTS	GDAS	PC-DARTS		ROME
			K=4	K=2	
Memory (G)	9.4	3.1	3.7	5.7	2.3

Table 3. Memory cost comparison. This evaluation is measured based on a batch size of 64, 16 initial channels, and 8 layers.

Models	Params	FLOPs	Error	Cost	SP
	(M)	(M)	(%)	GPU Days	
NASNet-A [42]	3.3	608 <sup>†</sup>	2.65	2000	✓
ENAS [25]	4.6	626 <sup>†</sup>	2.89	0.5	✓
DARTS-V1 [22]	3.3	528 <sup>†</sup>	3.00	0.4	×
SNAS [32]	2.8	422 <sup>†</sup>	2.85	1.5	×
P-DARTS [7]	3.4	532 <sup>†</sup>	2.50	0.2	×
PC-DARTS [33]	3.6	558 <sup>†</sup>	2.57	0.1	×
GDAS [12]	3.4	519 <sup>†</sup>	2.93	0.2	✓
ROME-v1-a	4.5	683	2.53	0.3	✓
<b>ROME-v2-a</b>	3.6	591	2.48	0.3	✓
DARTS-V1 [36]	-	-	3.38±0.23	0.4	×
P-DARTS [7] <sup>‡</sup>	3.3±0.2	540±34	2.81±0.14	0.3	×
PC-DARTS [33] <sup>‡</sup>	3.6±0.5	592±90	2.89±0.22	0.1	×
R-DARTS [38]	-	-	2.95±0.21	1.6	×
SDARTS-ADV [6]	3.3	-	2.61±0.02	1.3	×
ROME-v1	4.0±0.6	670±21	2.63±0.09	0.3	✓
<b>ROME-v2</b>	3.7±0.2	595±28	2.58±0.07	0.3	✓

Table 4. Performance comparisons on CIFAR-10. The first block reports the accuracy of the best model. The second block reports the averaged performance using 4 independent searches as recommended by [38, 6, 36]. <sup>‡</sup>: reproduced result using their released code since they didn't report the average performance. <sup>†</sup>: FLOPs is calculated by their released architecture. SP: single-path based method, which is memory-efficient.

on CIFAR-10. The average and standard deviation of the performance of our method are reported in Table 4, showing that ROME achieves state-of-the-art performance with only 0.3 GPU-days search cost<sup>3</sup>. Specifically, our best model achieves 97.52% accuracy with 3.6M parameters. Moreover, it's recommended to report average results across independent runs of searching [38, 6, 36, 9]. ROME-v2 achieves an average of 2.58±0.07% error rate, which slightly outperforms up-to-date SOTAs such as SDARTS-ADV [6]. However, ours takes 3× fewer time than it.

**Result on CIFAR-100.** We search on CIFAR-100 as [22] and show the results in Table 8 (supplementary). Our method also outperforms other SOTAs with a clear margin.

**Result on ImageNet.** As a common practice [22, 7, 18, 9], we transfer the architecture searched on CIFAR-10 to ImageNet. Following the same setting as [18, 9], we train models for 250 epochs with a batch size of 1024. Specifically, we utilize the SGD optimizer with 0.9 momentum. The learning rate is initialized as 0.5 and decayed by the cosine strategy. We also utilize cutout and 0.4 weighted aux-

<sup>3</sup>GDAS cost 0.2 GPU-days to search 250 epochs. We search 50 epochs with  $K = 7$ , being equivalent to search by GDAS for 350 epochs.

Models	FLOPs	Params	Top-1	Cost	Way
	(M)	(M)	(%)	(GPU days)	
AmoebaNet-A [26]	555	5.1	74.5	3150	TF
NASNet-A [42]	564	5.3	74.0	2000	TF
PNAS [21]	588	5.1	74.2	225	TF
DARTS [22]	574	4.7	73.3	0.4	TF
MdeNAS [39]	-	6.1	74.5	0.16	TF
PC-DARTS [33]	586	5.3	74.9	0.1	TF
FairDARTS-B [9]	541	4.8	75.1	0.4	TF
SNAS [32]	522	4.3	72.7	1.5	TF
GDAS [12]	581	5.3	74.0	0.2	TF
ROME-b (ours)	576	5.2	75.3	0.3	TF
PC-DARTS [33]	597	5.3	75.8	3.8	DS
FairNAS-C [8]	321	4.4	74.7	12	DS
SPOS [14]	323	3.5	74.4	12	DS
ProxylessNAS GPU [5]	465	7.1	75.1	8.3	DS
FBNet-C [31]	375	5.5	74.9	9	DS
GDAS* [12]	405	3.6	72.5	0.8	DS
ROME-c (ours)	556	5.1	75.5	0.5	DS

Table 5. Results on ImageNet. TF: transferred to ImageNet; DS: direct search on ImageNet. Our method can support direct search on large scale dataset for its memory efficiency. FBNet, FairNAS, SPOS and ProxylessNAS use a different search space as [28], which can achieve higher accuracy with fewer FLOPs. \*: obtained by our experiments based on the code publicly released by the authors.

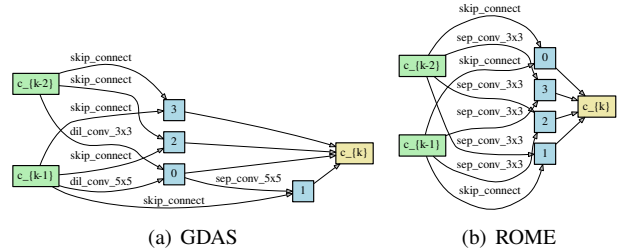


Figure 2. The architecture of normal cells searched by GDAS and ROME on ImageNet under S0 search space. Network searched by GDAS is dominated by skip connection and only obtains 72.5% accuracy on ImageNet, while our method is much more stable and achieves 75.5% accuracy.

iliary head loss. The result is shown in Table 5, our model ROME-b achieves 75.3% top-1 accuracy.

Moreover, ROME allows direct and proxyless search on ImageNet due to its low memory cost. We randomly sampling 10% and 10% images respectively from each class to train operation parameters and architecture weights. We construct a supernet by stacking 8 cells with 16 initial channels and search for 30 epochs with  $K = 3$ . The search time can be reduced to 0.4 GPU days on a single Tesla v100. The searched architecture (ROME-c in Table 5) is evaluated with the same training setting as above. As shown in Table 5, ROME-c achieves 75.5% top-1 accuracy on ImageNet validation set. To make fair comparisons, we also

Benchmark	DARTS <sup>†</sup>	R-DARTS <sup>†</sup>		DARTS <sup>†</sup>		SDARTS-RS <sup>†</sup>	ROME <sup>†</sup>		PC-DARTS <sup>‡</sup>	SDARTS-RS <sup>‡</sup>	ROME <sup>‡</sup>		
		DP	L2	ES	ADA		v1	v2			v1	v2	
C10	S1	3.84	3.11	2.78	3.01	3.10	2.78	<b>2.68</b>	<b>2.62</b>	3.11	2.78	<b>2.68</b>	<b>2.62</b>
	S2	4.85	3.48	3.31	3.26	3.35	3.33*	<b>3.24</b>	<b>2.95</b>	3.02	<b>2.75</b>	2.79	<b>2.62</b>
	S3	3.34	2.93	<b>2.51</b>	2.74	2.59	<b>2.53</b>	2.65	2.61	<b>2.51</b>	<b>2.53</b>	2.65	2.61
	S4	7.20	3.58	3.56	3.71	4.84	4.84*	<b>3.21</b>	<b>3.31</b>	3.02	<b>2.93</b>	3.61	<b>2.68</b>
C100	S1	29.46	25.93	24.25	28.37	24.03	23.51	22.34	<b>22.04</b>	18.87	<b>17.02</b>	17.27	<b>17.24</b>
	S2	26.05	22.30	22.24	23.25	23.52	22.28	<b>21.95</b>	<b>22.12</b>	18.23	17.56	<b>17.09</b>	<b>17.06</b>
	S3	28.90	22.36	23.99	23.73	23.37	<b>21.09</b>	22.56	<b>22.11</b>	18.05	17.73	<b>16.95</b>	<b>16.94</b>
	S4	22.85	22.18	21.94	<b>21.26</b>	23.20	21.46	21.33	<b>20.44</b>	17.16	17.17	<b>15.99</b>	<b>16.18</b>
SVHN	S1	4.58	2.55	4.79	2.72	2.53	2.35	<b>2.33</b>	<b>2.27</b>	2.28	2.26	<b>2.07</b>	<b>2.14</b>
	S2	3.53	2.52	2.51	2.60	2.54	2.39	<b>2.39</b>	<b>2.30</b>	2.39	2.37	<b>2.14</b>	<b>2.07</b>
	S3	3.51	2.49	<b>2.48</b>	2.50	2.50	<b>2.36</b>	2.58	2.51	2.27	2.21	<b>2.14</b>	<b>2.07</b>
	S4	3.05	2.61	2.50	2.51	2.46	2.46	<b>2.43</b>	<b>2.34</b>	2.37	2.35	<b>2.00</b>	<b>1.99</b>

Table 6. Comparison in RobustDARTS [38] reduced search spaces and 3 datasets. We report the **lowest error rate** of 3 found architectures. <sup>†</sup>: using the settings of [38] where CIFAR-100 and SVHN models have 8 layers and 16 initial channels, CIFAR-10 models have 20 layers and 36 initial channels except that S2 and S4 have 16 initial channels. \*: retrained with 16 initial channels. <sup>‡</sup>: using training settings where all models have 20 layers and 36 initial channels in [6]. The best is underlined and in bold face, the second best is in bold.

Benchmark		DARTS	DARTS-ES	DARTS-ADA	ROME-v1	ROME-v2
C10	S1	4.66±0.71	3.05±0.07	3.03±0.08	<b>2.93±0.09</b>	<b>2.66±0.06</b>
	S2	4.42±0.40	3.41±0.14	3.59±0.31	<b>3.34±0.12</b>	<b>3.14±0.14</b>
	S3	4.12±0.85	3.71±1.14	2.99±0.34	<b>2.72±0.09</b>	<b>2.61±0.00</b>
	S4	6.95±0.18	4.17±0.21	3.89±0.67	<b>3.21±0.00</b>	<b>3.44±0.12</b>
C100	S1	29.93±0.41	28.90±0.81	24.94±0.81	<b>22.65±0.45</b>	<b>22.71±0.71</b>
	S2	28.75±0.92	24.68±1.43	26.88±1.11	<b>23.14±0.98</b>	<b>22.91±0.75</b>
	S3	29.01±0.24	26.99±1.79	24.55±0.63	<b>23.03±0.66</b>	<b>22.43±0.36</b>
	S4	24.77±1.51	23.90±2.01	23.66±0.90	<b>21.33±0.00</b>	<b>20.95±0.45</b>
SVHN	S1	9.88±5.50	2.80±0.09	2.59±0.07	<b>2.37±0.04</b>	<b>2.34±0.06</b>
	S2	3.69±0.12	2.68±0.18	2.79±0.22	<b>2.49±0.14</b>	<b>2.41±0.07</b>
	S3	4.00±1.01	2.78±0.29	<b>2.58±0.07</b>	2.61±0.03	<b>2.56±0.03</b>
	S4	2.90±0.02	2.55±0.15	2.52±0.06	<b>2.43±0.00</b>	<b>2.34±0.00</b>

Table 7. Comparison in 4 search spaces and 3 datasets. We report the mean and variance about **lowest error rate** of 3 found architectures. We use the model settings as in [38]. In case the variance is zero, it means that we found three identical networks.

search for 90 epochs by GDAS [12] under the same settings. However, the network is dominated by skip connection and only achieves 72.5% top-1 accuracy. The structure of normal cells searched by GDAS and ROME are shown in Fig. 2. The structure of reduction cells are shown in the supplementary ( Fig. 6 and Fig. 7).

#### 4.4. Robustness Evaluation on 12 Benchmarks

We further evaluate the performance and generalization of our method on recent 4 harder search spaces across 3 datasets from [38]. For each benchmark, we perform four independent searches and train the searched 4 models to report their performance by mean and standard variance. This process is recommended by [34, 6, 38] to fairly compare different NAS methods. The result is shown in Table 7. Our methods robustly outperform RobustDARTS with a clear margin across the 12 benchmarks with 3× fewer search cost. The best cells found by ROME v1 and v2 are shown in Sec. C in the supplementary material.

## 4.5. Discussions

**Memory cost comparison with PC-DARTS.** PC-DARTS utilizes partial channels during the search stage to reduce GPU memory cost, in which the partial ratio is controlled by a hyperparameter  $K$ .  $K$  requires careful calibration for different tasks. Moreover, it still needs a partial whole supernet to perform the search. Given a mixed micro operator with  $N$  candidate operations, the memory cost is  $\mathcal{O}(KN)$ . In contrast, ours doesn’t require calibrating such an extra hyperparameter and enjoys a cost of  $\mathcal{O}(1)$ .

**Discussion on collapse behavior across popular NAS benchmarks.** We argue that excluding an important operation for search space can cause illusive conclusions. Specifically, NAS-Bench-1Shot1 [2] suggests that Gumbel-based NAS is quite robust. However, this observation is laying on the basis that popular skip connections are not included in the search space [35]. After adding skip connection into the choices, we perform the GDAS search using their released code<sup>4</sup>. The best model found is full of skip connections, which again supports our discovery of collapse issue in single-path based NAS, see Fig. 3 and more in Fig. 15 in the supplemental material. Instead, while performing ROME-v2 in such modified search spaces, we don’t suffer the same issue, see Fig. 16 in the supplemental material.

## 5. Conclusion

In this paper, we highlight a new performance collapse of single-path NAS paradigm based on Gumbel reparameterization, and attribute it to inconsistent searching for topology and stochastic nature of sampling candidate operations. Therefore, we propose topology disentanglement for consistent search and gradient accumulation mechanism to re-

<sup>4</sup><https://github.com/automl/nasbench-1shot1>



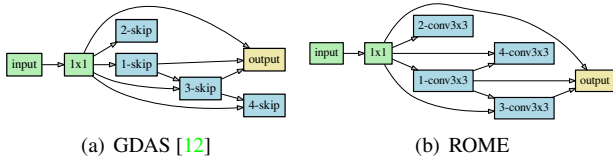


Figure 3. GDAS fails on NAS-Bench-1Shot1 [2] on CIFAR-10 when adding skip connection to the second search space. Notice that nodes with no out-degrees have no contribution to the output.

duce the sampling variance. Unlike the previous single-path based works that suffer from instability issue, our method robustly achieves state-of-the-art results across 15 recent popular benchmarks.

## References

- [1] G Anandalingam and Terry L Friesz. Hierarchical optimization: An introduction. *Annals of Operations Research*, 34(1):1–11, 1992. 2
- [2] Zela Arber, Siems Julien, and Hutter Frank. Nas-bench-1shot1: Benchmarking and dissecting one-shot neural architecture search. In *ICLR*, 2020. 8, 9, 16, 17
- [3] Gabriel Bender, Pieter-Jan Kindermans, Barret Zoph, Vijay Vasudevan, and Quoc Le. Understanding and Simplifying One-Shot Architecture Search. In *ICML*, pages 549–558, 2018. 1
- [4] Andrew Brock, Theodore Lim, James M Ritchie, and Nick Weston. SMASH: One-Shot Model Architecture. Search Through HyperNetworks. In *ICLR*, 2018. 1
- [5] Han Cai, Ligeng Zhu, and Song Han. ProxylessNAS: Direct Neural Architecture Search on Target Task and Hardware. In *ICLR*, 2019. 1, 2, 7
- [6] Xiangning Chen and Cho-Jui Hsieh. Stabilizing differentiable architecture search via perturbation-based regularization. In *ICML*, 2020. 1, 2, 3, 6, 7, 8
- [7] Xin Chen, Lingxi Xie, Jun Wu, and Qi Tian. Progressive Differentiable Architecture Search: Bridging the Depth Gap between Search and Evaluation. In *ICCV*, 2019. 1, 2, 6, 7, 11
- [8] Xiangxiang Chu, Bo Zhang, Ruijun Xu, and Jixiang Li. FairNAS: Rethinking Evaluation Fairness of Weight Sharing Neural Architecture Search. *arXiv preprint arXiv:1907.01845*, 2019. 2, 7
- [9] Xiangxiang Chu, Tianbao Zhou, Bo Zhang, and Jixiang Li. Fair darts: Eliminating unfair advantages in differentiable architecture search. *ECCV*, 2020. 2, 3, 7
- [10] Jia Deng, Wei Dong, Richard Socher, Li-Jia Li, Kai Li, and Li Fei-Fei. ImageNet: A Large-Scale Hierarchical Image Database. In *CVPR*, pages 248–255. IEEE, 2009. 6
- [11] Xuanyi Dong and Yi Yang. One-shot neural architecture search via self-evaluated template network. In *ICCV*, pages 3681–3690, 2019. 2
- [12] Xuanyi Dong and Yi Yang. Searching for a Robust Neural Architecture in Four GPU Hours. In *CVPR*, pages 1761–1770, 2019. 1, 2, 3, 4, 5, 7, 8, 9, 11
- [13] Golnaz Ghiasi, Tsung-Yi Lin, and Quoc V Le. Nas-fpn: Learning scalable feature pyramid architecture for object detection. In *CVPR*, pages 7036–7045, 2019. 1
- [14] Zichao Guo, Xiangyu Zhang, Haoyuan Mu, Wen Heng, Zechun Liu, Yichen Wei, and Jian Sun. Single Path One-Shot Neural Architecture Search with Uniform Sampling. In *ECCV*, 2020. 2, 7
- [15] Andrew Howard, Mark Sandler, Grace Chu, Liang-Chieh Chen, Bo Chen, Mingxing Tan, Weijun Wang, Yukun Zhu, Ruoming Pang, Vijay Vasudevan, et al. Searching for MobileNetV3. In *ICCV*, 2019. 1
- [16] Eric Jang, Shixiang Gu, and Ben Poole. Categorical reparameterization with gumbel-softmax. In *International Conference on Learning Representations*, 2016. 1
- [17] Alex Krizhevsky, Geoffrey Hinton, et al. Learning Multiple Layers of Features from Tiny Images. Technical report, Citeseer, 2009. 6
- [18] Guohao Li, Guocheng Qian, Itzel C Delgadillo, Matthias Müller, Ali Thabet, and Bernard Ghanem. Sgas: Sequential greedy architecture search. In *CVPR*, 2020. 7
- [19] Hanwen Liang, Shifeng Zhang, Jiacheng Sun, Xingqiu He, Weiran Huang, Kechen Zhuang, and Zhenguo Li. Darts+: Improved differentiable architecture search with early stopping. *arXiv preprint arXiv:1909.06035*, 2019. 1, 2
- [20] Chenxi Liu, Liang-Chieh Chen, Florian Schroff, Hartwig Adam, Wei Hua, Alan L Yuille, and Li Fei-Fei. Auto-deeplab: Hierarchical neural architecture search for semantic image segmentation. In *CVPR*, pages 82–92, 2019. 1
- [21] Chenxi Liu, Barret Zoph, Maxim Neumann, Jonathon Shlens, Wei Hua, Li-Jia Li, Li Fei-Fei, Alan Yuille, Jonathan Huang, and Kevin Murphy. Progressive Neural Architecture Search. In *ECCV*, pages 19–34, 2018. 7, 11
- [22] Hanxiao Liu, Karen Simonyan, and Yiming Yang. DARTS: Differentiable Architecture Search. In *ICLR*, 2019. 1, 2, 5, 6, 7, 11
- [23] Chris J Maddison, Andriy Mnih, and Yee Whye Teh. The concrete distribution: A continuous relaxation of discrete random variables. *arXiv preprint arXiv:1611.00712*, 2016. 1
- [24] Yuval Netzer, Tao Wang, Adam Coates, Alessandro Bisacco, Bo Wu, and Andrew Y. Ng. Reading digits in natural images with unsupervised feature learning. In *NIPSW*, 2011. 6
- [25] Hieu Pham, Melody Y Guan, Barret Zoph, Quoc V Le, and Jeff Dean. Efficient Neural Architecture Search via Parameter Sharing. In *ICML*, 2018. 1, 2, 7, 11
- [26] Esteban Real, Alok Aggarwal, Yanping Huang, and Quoc V Le. Regularized evolution for image classifier architecture search. In *AAAI*, volume 33, pages 4780–4789, 2019. 7, 11
- [27] Dimitrios Stamoulis, Ruizhou Ding, Di Wang, Dimitrios Lymberopoulos, Bodhi Priyantha, Jie Liu, and Diana Marculescu. Single-Path NAS: Designing Hardware-Efficient ConvNets in less than 4 Hours. *ECML PKDD*, 2019. 1, 2
- [28] Mingxing Tan, Bo Chen, Ruoming Pang, Vijay Vasudevan, and Quoc V Le. Mnasnet: Platform-Aware Neural Architecture Search for Mobile. In *CVPR*, 2019. 1, 7

- [29] Mingxing Tan and Quoc V Le. EfficientNet: Rethinking Model Scaling for Convolutional Neural Networks. In *ICML*, 2019. 1
- [30] Xiaoxing Wang, Chao Xue, Junchi Yan, Xiaokang Yang, Yonggang Hu, and Kewei Sun. Mergenas: Merge operations into one for differentiable architecture search. In *International Joint Conference on Artificial Intelligence*, 2020. 2
- [31] Bichen Wu, Xiaoliang Dai, Peizhao Zhang, Yanghan Wang, Fei Sun, Yiming Wu, Yuandong Tian, Peter Vajda, Yangqing Jia, and Kurt Keutzer. FBNet: Hardware-Aware Efficient ConvNet Design via Differentiable Neural Architecture Search. In *CVPR*, 2019. 1, 3, 7
- [32] Sirui Xie, Hehui Zheng, Chunxiao Liu, and Liang Lin. SNAS: Stochastic Neural Architecture Search. In *ICLR*, 2019. 1, 3, 4, 7
- [33] Yuhui Xu, Lingxi Xie, Xiaopeng Zhang, Xin Chen, Guo-Jun Qi, Qi Tian, and Hongkai Xiong. Pc-darts: Partial channel connections for memory-efficient architecture search. In *ICLR*, 2020. 2, 7
- [34] Antoine Yang, Pedro M. Esperança, and Fabio M. Carlucci. Nas evaluation is frustratingly hard. In *International Conference on Learning Representations*, 2020. 8
- [35] Chris Ying, Aaron Klein, Eric Christiansen, Esteban Real, Kevin Murphy, and Frank Hutter. NAS-bench-101: Towards reproducible neural architecture search. In Kamalika Chaudhuri and Ruslan Salakhutdinov, editors, *Proceedings of the 36th International Conference on Machine Learning*, volume 97 of *Proceedings of Machine Learning Research*, pages 7105–7114, Long Beach, California, USA, 09–15 Jun 2019. PMLR. 8
- [36] Kaicheng Yu, Christian Sciuto, Martin Jaggi, Claudiu Musat, and Mathieu Salzmann. Evaluating the search phase of neural architecture search. In *ICLR*, 2020. 7
- [37] Arber Zela, Thomas Elsken, Tonmoy Saikia, Yassine Marrakchi, Thomas Brox, and Frank Hutter. Understanding and Robustifying Differentiable Architecture Search. In *ICLR*, 2020. 1
- [38] Arber Zela, Thomas Elsken, Tonmoy Saikia, Yassine Marrakchi, Thomas Brox, and Frank Hutter. Understanding and robustifying differentiable architecture search. In *ICLR*, 2020. 1, 2, 3, 6, 7, 8, 11
- [39] Xiawu Zheng, Rongrong Ji, Lang Tang, Baochang Zhang, Jianzhuang Liu, and Qi Tian. Multinomial Distribution Learning for Effective Neural Architecture Search. In *ICCV*, pages 1304–1313, 2019. 7
- [40] Pan Zhou, Caiming Xiong, Richard Socher, and Steven Hoi. Theory-inspired path-regularized differential network architecture search. In *Neural Information Processing Systems*, 2020. 3
- [41] Barret Zoph and Quoc V Le. Neural Architecture Search with Reinforcement Learning. In *ICLR*, 2017. 1
- [42] Barret Zoph, Vijay Vasudevan, Jonathon Shlens, and Quoc V Le. Learning Transferable Architectures for Scalable Image Recognition. In *CVPR*, volume 2, 2018. 2, 7

## A. Proof of Gumbel Max Two Process

This section will prove that the sampling scheme proposed in ROME-v2 is equivalent to sample two different edges without replacement with the probability simplex  $p_i = \frac{\exp \beta_i}{\sum_{i'} \exp(\beta_{i'})}$ .

Let  $p_i$  be the probability of  $i$ -th edge being selected by single choice. In such selecting scheme, the results that it was chosen among  $n$  edges can be divided in to two parts. Without loss of generality, we discuss about the first edge's being chosen.

**A** It is selected by the first choice, and the probability is  $p_1$ .

**B** It is selected by the second choice, and the probability is  $\sum_{i=2}^n p_i \frac{p_1}{1-p_i}$ , where  $\frac{p_1}{1-p_i}$  is the scaled probability when take  $i$  away without putting back.

Let's talk about gumbel max scheme, in which we sample  $n$  real numbers  $\epsilon_i$  from  $U[0, 1]$  and choose the max two  $\log p_i - \log(-\log \epsilon_i)$ s. There are also two kinds results here.

**A**  $\log p_1 - \log(-\log \epsilon_1)$  is the biggest one, and the probability is  $p_1$ .

**B**  $\log p_1 - \log(-\log \epsilon_1)$  is the second biggest one only next to  $\log p_i - \log(-\log \epsilon_i)$ . That is

$$\begin{aligned} \log p_1 - \log(-\log \epsilon_1) &> \log p_2 - \log(-\log \epsilon_2) \\ \log p_1 - \log(-\log \epsilon_1) &> \log p_3 - \log(-\log \epsilon_3) \\ &\dots \\ \log p_1 - \log(-\log \epsilon_1) &< \log p_i - \log(-\log \epsilon_i) \\ &\dots \\ \log p_1 - \log(-\log \epsilon_1) &> \log p_n - \log(-\log \epsilon_n). \end{aligned}$$

Notably, these  $n - 1$  events are mutually independent. Therefore, it can be expressed as

$$\begin{aligned} \epsilon_2 &< \epsilon_1^{p_2/p_1} \\ &\dots \\ \epsilon_1^{p_i/p_1} &< \epsilon_i \\ &\dots \\ \epsilon_n &< \epsilon_1^{p_n/p_1}. \end{aligned}$$

Because *epsilons* are sampled uniformly from zero to one, we directly get the probability of all these events above happening together.

$$\begin{aligned} P &= \epsilon_1^{p_2/p_1} \epsilon_1^{p_3/p_1} \dots (1 - \epsilon_1^{p_i/p_1}) \dots \epsilon_1^{p_n/p_1} \\ &= (1 - \epsilon_1^{p_i/p_1}) \epsilon_1^{\frac{1-p_i}{p_1} - 1}. \end{aligned}$$

Models	Params (M)	Error (%)	Cost GPU Days
ResNet [?]	1.7	22.10 <sup>◊</sup>	-
AmoebaNet [26]	3.1	18.93 <sup>◊</sup>	3150
PNAS [21]	3.2	19.53 <sup>◊</sup>	150
ENAS [25]	4.6	19.43 <sup>◊</sup>	0.45
DARTS [22]	-	20.58±0.44*	0.4
GDAS [12]	3.4	18.38	0.2
P-DARTS [7]	3.6	17.49 <sup>‡</sup>	0.3
R-DARTS [38]	-	18.01±0.26	1.6
ROME-V1 (avg.)	4.4±0.2	17.41±0.12	0.3
ROME-V1 (best)	4.4	17.33	0.3
ROME-V2 (avg.)	3.4	17.71±0.11	0.3
ROME-V2 (best)	3.3	17.57	0.3

Table 8. Comparison of searched models on CIFAR-100. <sup>◊</sup>: Reported by [12], \*: Reported by [38], <sup>‡</sup>:Rerun their code.

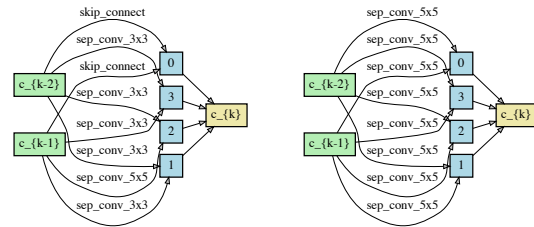


Figure 4. Best normal and reduction by ROME-v1 on CIFAR-10.

Integrate  $\epsilon_1$  across its domain,

$$\begin{aligned} &\int_0^1 (1 - \epsilon_1^{p_i/p_1}) \epsilon_1^{\frac{1-p_i}{p_1} - 1} d\epsilon_1 \\ &= \int_0^1 \epsilon_1^{\frac{1-p_i}{p_1} - 1} - \epsilon_1^{\frac{1}{p_1} - 1} d\epsilon_1 \\ &= \frac{p_1}{1 - p_i} - p_1 = p_i \frac{p_1}{1 - p_i} \end{aligned}$$

which meets the equation before.

## B. Further Experiments

Table 8 gives CIFAR-100 results.

## C. Figures of Genotypes

Genotypes are list in Figure 4 to 16.

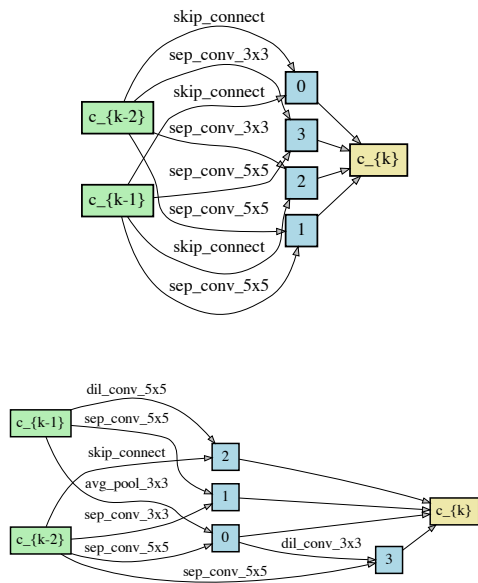


Figure 5. Best normal and reduction by ROME-v2 on CIFAR-10.

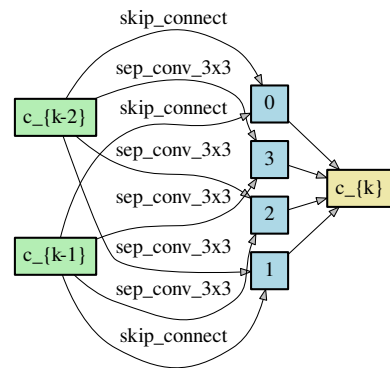


Figure 7. The best architecture found by ROME on ImageNet in S0. No performance collapse occurs.

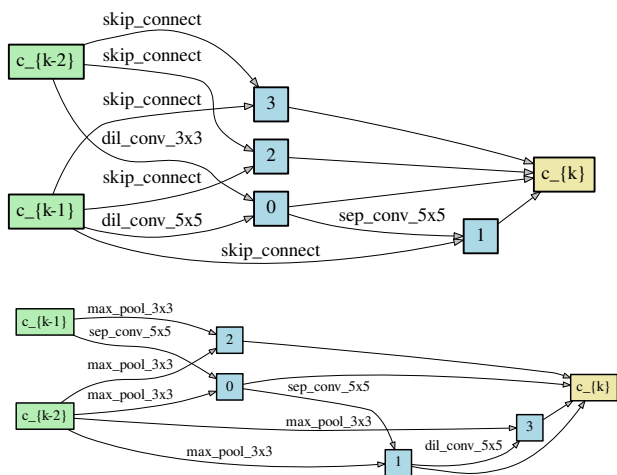


Figure 6. The best architecture found by GDAS on ImageNet in S0. Skip connection dominate the searched architecture.

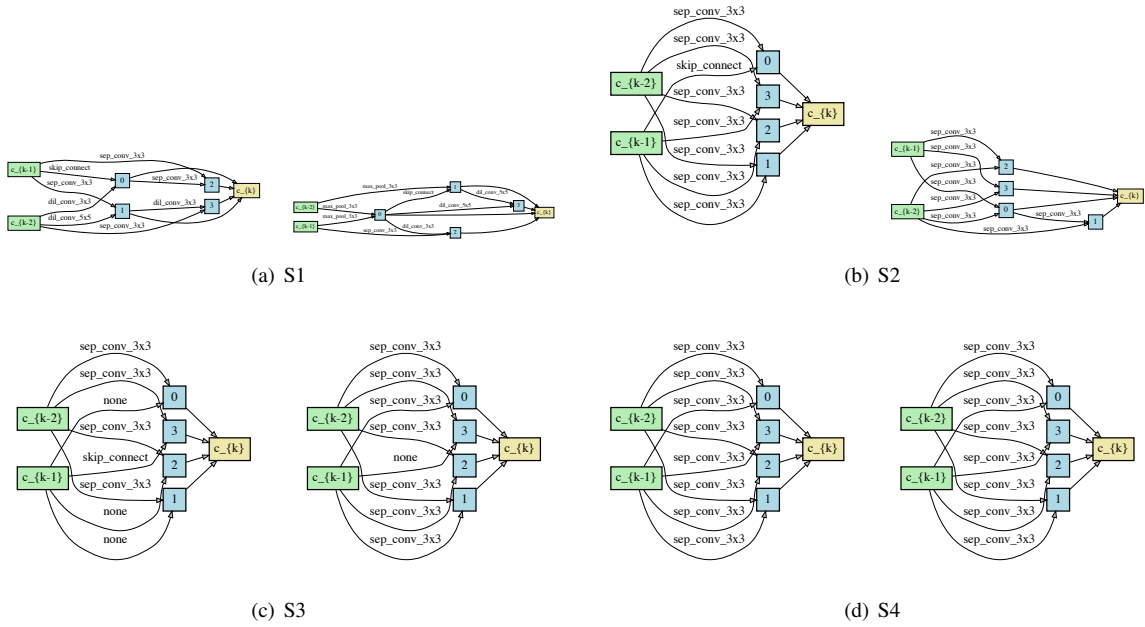


Figure 8. ROME-V1 best cells (paired in normal and reduction) on CIFAR10 in reduced search spaces of RobustDARTS.

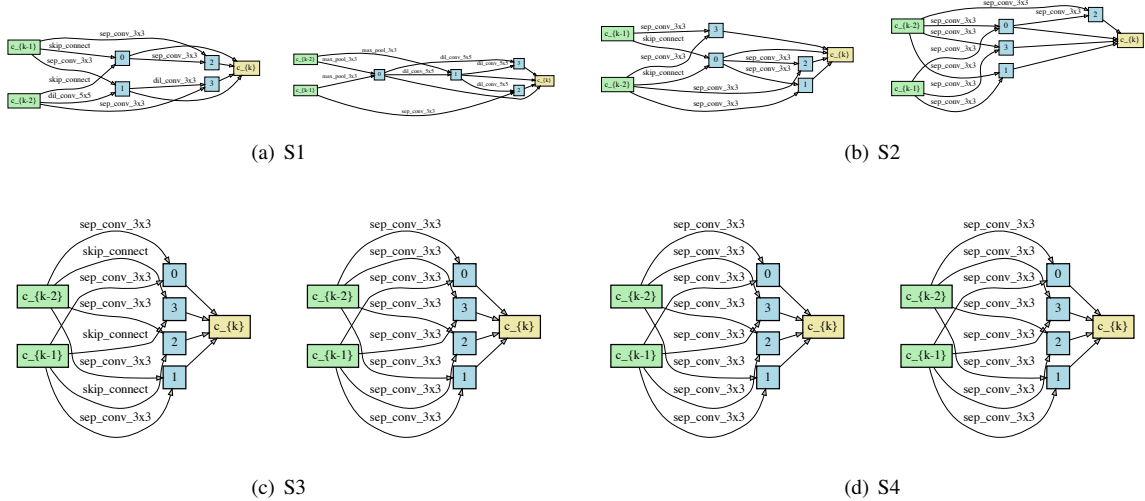


Figure 9. ROME-V1 best cells (paired in normal and reduction) on CIFAR100 in reduced search spaces of RobustDARTS.

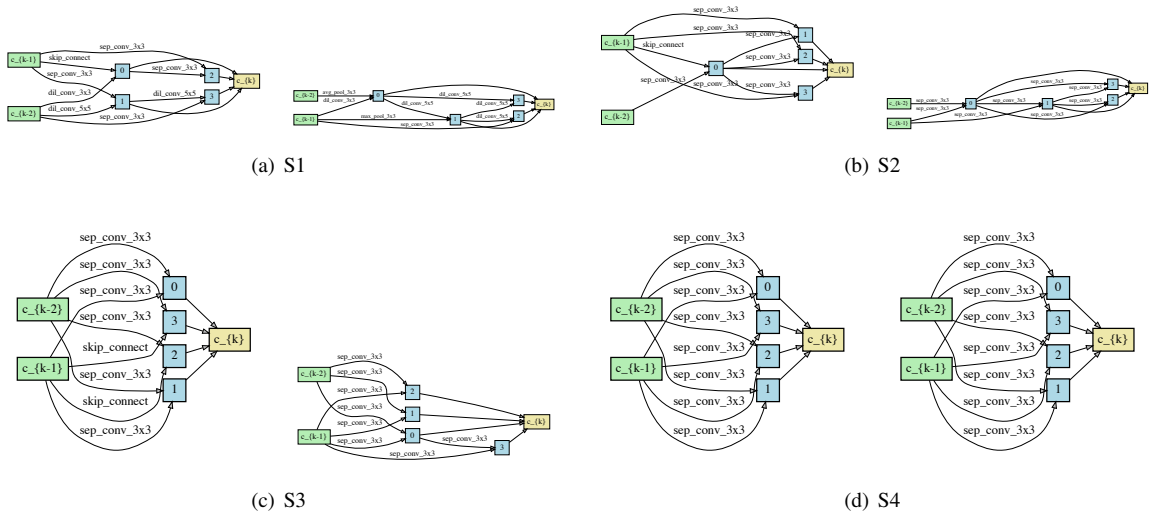


Figure 10. ROME-V1 best cells (paired in normal and reduction) on SVHN in reduced search spaces of RobustDARTS.

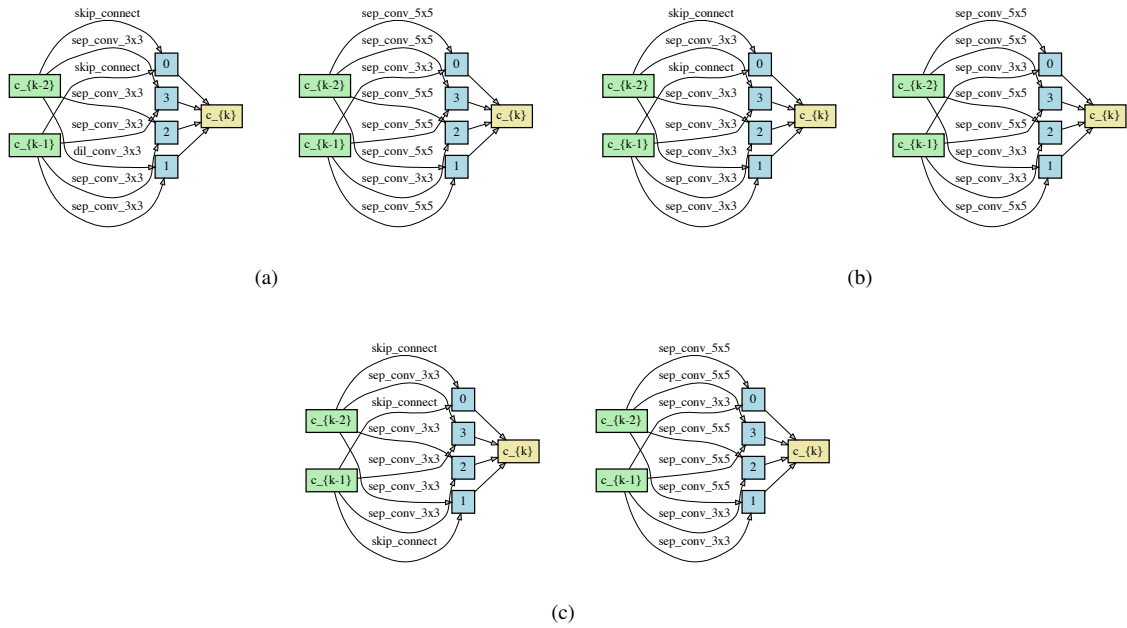


Figure 11. ROME-V1 cells (paired in normal and reduction) on CIFAR-100 in DARTS's search space.

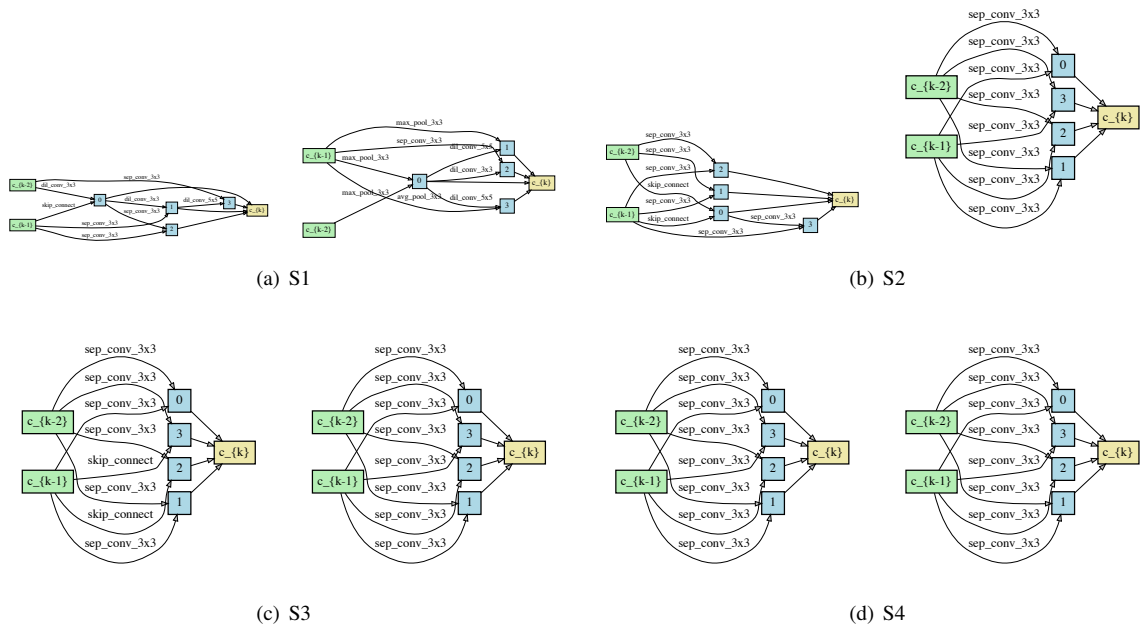


Figure 12. ROME-V2 best cells (paired in normal and reduction) on CIFAR10 in reduced search spaces of RobustDARTS.

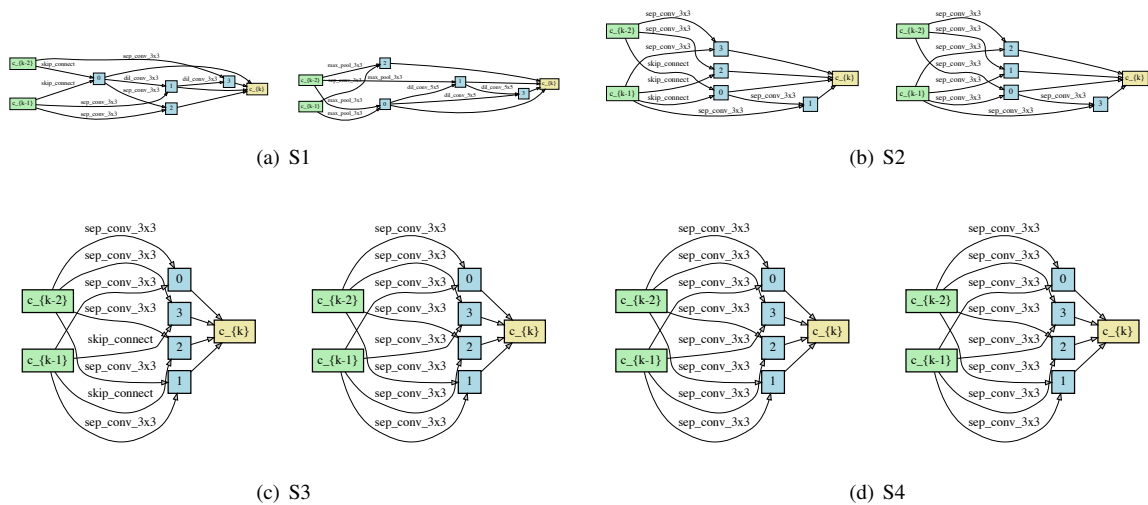


Figure 13. ROME-V2 best cells (paired in normal and reduction) on CIFAR100 in reduced search spaces of RobustDARTS.

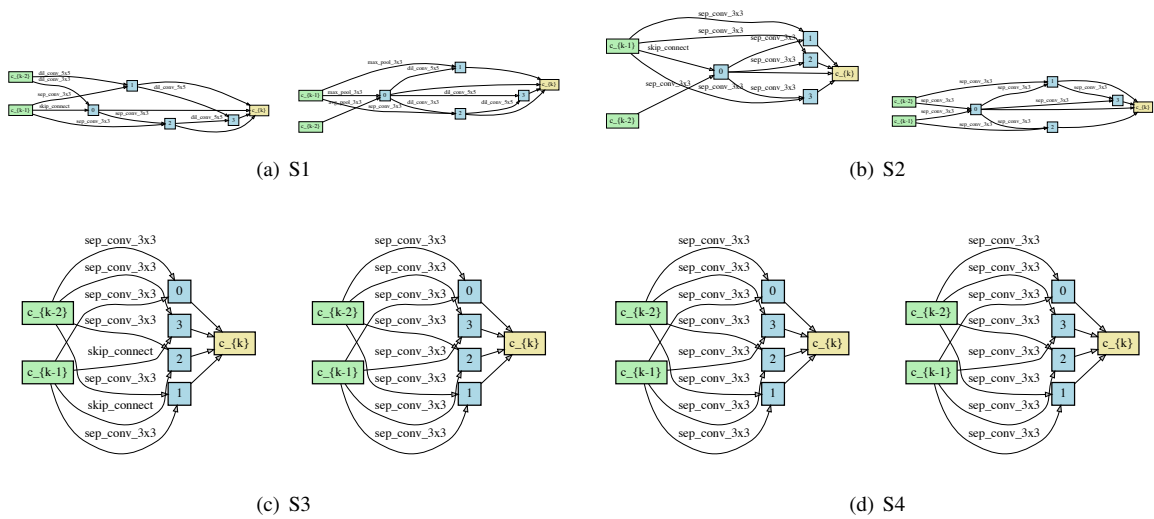


Figure 14. ROME-V2 best cells (paired in normal and reduction) on SVHN in reduced search spaces of RobustDARTS.

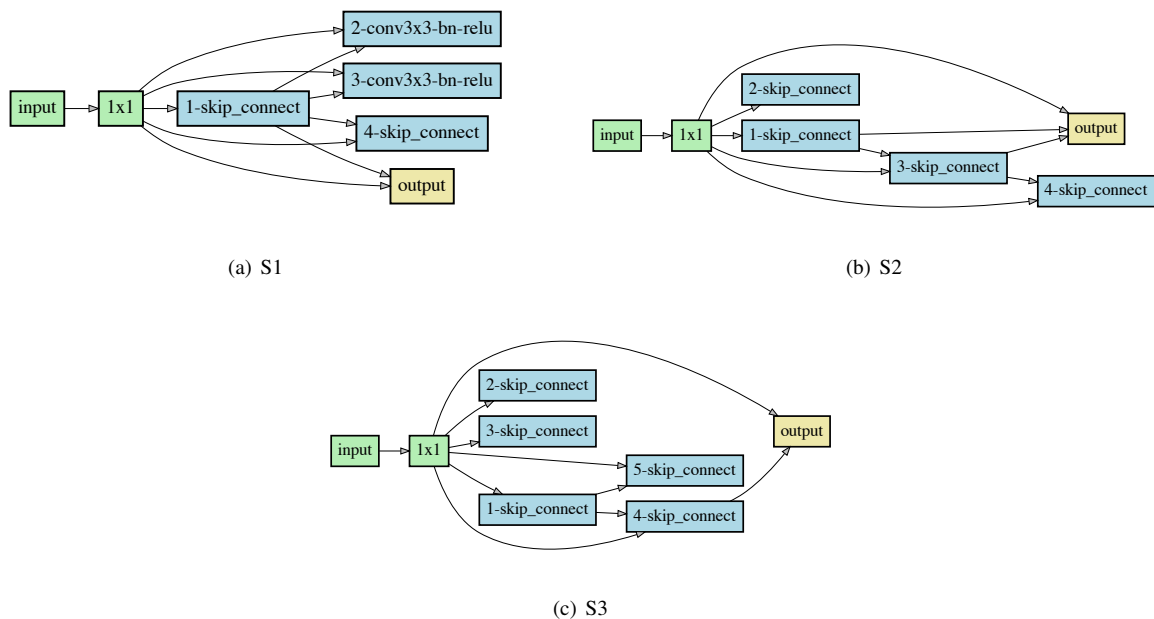


Figure 15. GDAS fails on NAS-Bench-1Shot1 [2] when searching on CIFAR-10 in all three search spaces when skip connection are added into choices. In each MixedOp, we have three choices:  $\{\text{maxpool3x3}, \text{conv3x3-bn-relu}, \text{skip-connect}\}$ .



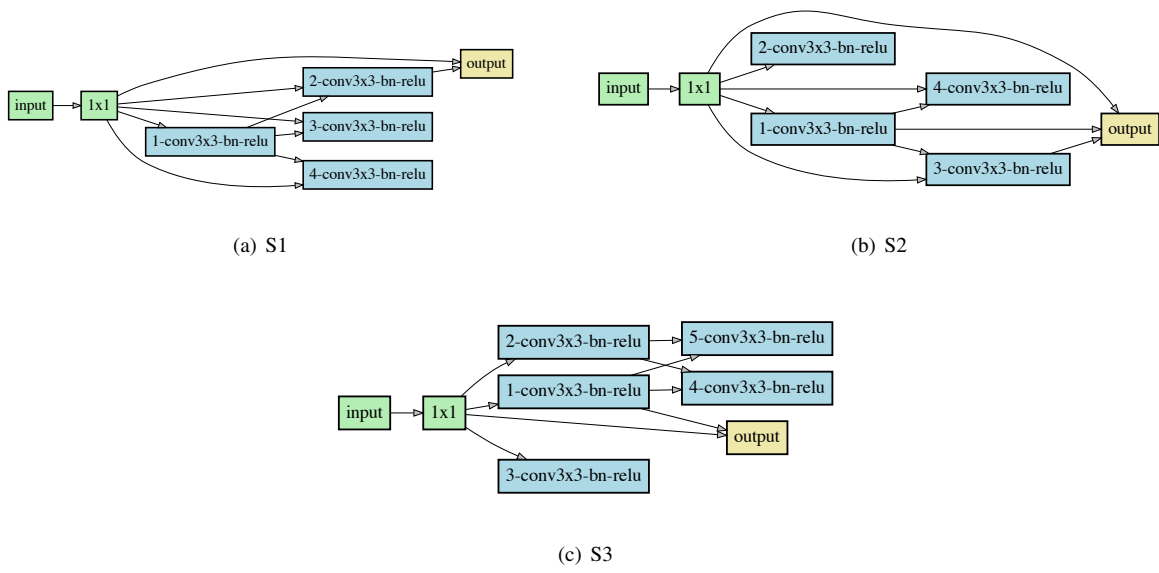


Figure 16. ROME-V2 resolves the aggregation of skip connections on NAS-Bench-1Shot1 [2]. Notice intermediate nodes concatenate their outputs as the input for the output node, while some have loose ends and don't feed to the output node.